Laser Physics Letters

Astro Ltd.

LETTER

Multi-mode correlation with self- and cross-Rabi oscillation in a diamond nitrogen-vacancy center

To cite this article: Faizan Raza *et al* 2019 *Laser Phys. Lett.* **16** 055402

IOP Publishing | Astro Ltd
Laser Physics Letters
Laser Phys. Lett. **16** (2019) 055402 (5pp)
https://doi.org/10.1088/1612-202X/ab126b

Letter

Multi-mode correlation with self- and cross-Rabi oscillation in a diamond nitrogen-vacancy center

Faizan Raza[1], Al Imran[1], Xinghua Li[1], Wei Li[1], Yameng Li[1], Jianyong Mao[1] and Yanpeng Zhang[1]

[1] Key Laboratory for Physical Electronics and Devices of the Ministry of Education and Shaanxi Key Lab of Information Photonic Technique, Xi'an Jiaotong University, Xi'an 710049, People's Republic of China

E-mail: ypzhang@mail.xjtu.edu.cn

Received 14 December 2018
Accepted for publication 5 March 2019
Published 10 April 2019

Abstract

Here we report on the damped cross-Rabi oscillations in the intensity noise correlation resulting from the destructive interference between two four-wave mixing (FWM) processes, controlled by dressing atomic coherence in a nitrogen-vacancy center in a diamond. Also, the relationship between the self-Rabi oscillation of temporal intensity and cross-Rabi oscillation is investigated at a low temperature. Additionally, we discuss the notion that cross-Rabi oscillation in correlated beams can be switched between FWM and second-order fluorescence.

Keywords: nonlinear optics, nitrogen vacancy center in diamond, fourwave mixing, Rabi oscillations

(Some figures may appear in colour only in the online journal)

1. Introduction

Four-wave mixing (FWM) is a remarkable phenomenon in non-linear optics, in which two frequencies ω_1 and ω_2 interact and produce a new pair of frequencies: ω_{AS} and ω_S. Using electromagnetically induced transparency [1], FWM has even been studied at a low-light level [2]. Entangled paired photons explore an extraordinary area of research in physics, like quantum information processing [3]. Entangled photon pairs or biphotons have many attractive applications in quantum computing and communication [4], and spectroscopy [5]. The space-time entangled biphoton state generated from a two-level atomic system using magneto-optically trapped cold ^{87}Rb atomic ensembles are discussed [6]. In three-level systems, the interference of degenerate FWM has been studied in both quantum and classical regimes [7]. Recently, the coincidence counting rate of paired photons generated from a two-level atomic system exhibits a damped Rabi oscillation and a photon antibunching-like effect [6, 8]. Rabi oscillation and the photon antibunching-like effect originate from the destructive interference between two different types of FWMs.

The negatively charged nitrogen-vacancy (NV^-) center in a diamond is an individually addressable electronic spin that can be initialized and read out optically at room temperature [9]. The NV^- has quite a high signal-to-background ratio, which ensures that a single bit of information is encoded in a single photon [10]. The NV^- center has an electron spin coherence time in milliseconds [11], credited to the low phonon density of the states and the stability of the host material [12], inspiring a broad range of compelling applications in solid state quantum computation [13]. Quantum lithography beyond the diffraction limit is also achieved via Rabi oscillations [14]. Photon interference among distant non-classical emitters is a promising method to generate large scale quantum networks. Biphoton interference is best achieved when photons show long coherence times. The NV defect center in the diamond coherence time of a photon is very large and can be manipulated via Rabi oscillations, which makes them an ideal

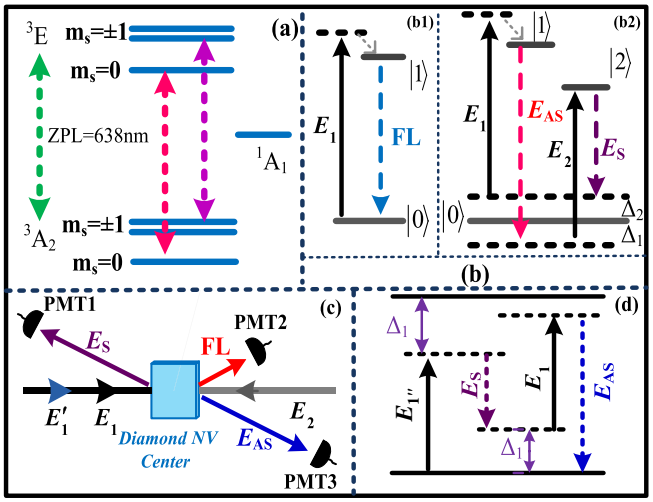

Figure 1. (a) The energy level structure of NV^- with triplet excited and ground states associated with intermediate metastable singlet state. (b) The energy levels of the NV center. (b1) Two- and (b2) V-type energy levels of the NV center. (c) Experimental setup scheme and laser coupling configuration. (d) FWM in a two-level system.

candidate for designing quantum networks [15]. We have discussed the cross-Rabi oscillation from the destructive interference between two FWM processes, controlled by the dressing field in an atomic-like system.

In this paper, we report the temporal intensity of self- and cross-Rabi oscillation in correlated light beams from a spontaneous parametric four-wave mixing (SPFWM) process in an NV^-. Meanwhile, we established the relationship between the temporal intensity of self- and cross-Rabi oscillations.

2. Experimental setup

The sample used in our experiment was a bulk NV center crystal, consisting of substitutional nitrogen-lattice vacancy pairs, orientated along the [1 0 0] crystalline direction. The sample used in our experiment contains 0.05% nitrogen per diamond crystal. The sample was held in cryostat; the cryostat temperature was maintained at 77 K by flowing liquid nitrogen. Figure 1(b) shows the energy level scheme of the NV^-. The NV^- has two triplet states; named the ground state $^3A_2$ and the excited state ^3E, and two singlet states ($^1A_1$, ^1E). The two triplet states $^3A_2$ and ^3E are split into $|m_s = 0\rangle$ and $|m_s = \pm 1\rangle$ fine-structure levels. The energy difference between $|m_s = 0\rangle$ and $|m_s = \pm 1\rangle$ for $^3A_2$ is $D = 2.8$ GHz, while, for the excited state, ^3E is $D = 1.42$ GHz [16].

Figure 1(c) shows the schematic diagram of the experimental setup. Two dye lasers (narrow scan with a 0.04 cm^{-1} linewidth) pumped by an injection locked single-mode Nd:YAG laser (Continuum Powerlite DLS 9010, 10 Hz repetition rate, 5 ns pulse width) are used to generate the pumping fields $\boldsymbol{E_1}$ (ω_1, Δ_1) and $\boldsymbol{E_2}$ (ω_2, Δ_2) with frequency detuning $\Delta_i = \Omega_{mn} - \omega_i$, where Ω_{mn} is the corresponding atomic transition frequency between levels $|m\rangle$ and $|n\rangle$, and ω_i ($i = 1, 2$) is the laser frequency. The pumping fields $\boldsymbol{E_1}$ and $\boldsymbol{E_2}$ satisfy the phase-matching condition $\boldsymbol{k_1} + \boldsymbol{k_2} = \boldsymbol{k_S} + \boldsymbol{k_{AS}}$, where $i = 1, 2$ and $\boldsymbol{k}$ are the wavevectors of the pumping fields and the generated photon pairs. $\boldsymbol{E_1}$ and $\boldsymbol{E_2}$ are coupled to the transitions $(|0\rangle) \leftrightarrow (|1\rangle)$ and $(|0\rangle) \leftrightarrow (|2\rangle)$, respectively. Arrangements of three photomultiplier tubes (PMT1-3) are used to detect the generated $\boldsymbol{E_S}$, $\boldsymbol{E_{AS}}$ and FL composite signals (figure 1(c)).

By the opening fields $\boldsymbol{E_1}$ and $\boldsymbol{E_2}$, the anti-Stokes $\boldsymbol{E_{AS}}$ and Stokes signals $\boldsymbol{E_S}$ are generated with phase-matching conditions $\boldsymbol{k_{AS}} = \boldsymbol{k_1} + \boldsymbol{k_2} - \boldsymbol{k_S}$ and $\boldsymbol{k_S} = \boldsymbol{k_1} + \boldsymbol{k_2} - \boldsymbol{k_{AS}}$, respectively. The perturbation chains for the $\boldsymbol{E_S}$ and $\boldsymbol{E_{AS}}$ signals in the V-type three-level system are written as $\rho_{00}^{(0)} \xrightarrow{E_1} \rho_{10}^{(1)} \xrightarrow{E_{AS}} \rho_{00}^{(2)} \xrightarrow{E_2} \rho_{20(S)}^{(3)}$ and $\rho_{00}^{(0)} \xrightarrow{E_1} \rho_{10}^{(1)} \xrightarrow{E_{AS}} \rho_{00}^{(2)} \xrightarrow{E_2} \rho_{20(S)}^{(3)}$, respectively. The third order nonlinear density matrix elements of the SPFWM signals via the perturbation chains are given as [17, 18]

$$\rho_{10}^{(3)} = \frac{-iG_S G_1 G_2}{(\Gamma_{20} + i\Delta_2)(\Gamma_{00} + i\delta)(\Gamma_{10} - i\delta + \Delta_1 + |G_1|^2/\Gamma_{00} - i\delta + d_1)} \tag{1}$$

$$\rho_{20}^{(3)} = \frac{-iG_{AS} G_1 G_2}{(\Gamma_{10} + i\Delta_1)(\Gamma_{20} + i\delta + i\Delta_2)(\Gamma_{00} + i\delta + |G_1|^2/\Gamma_{00} - i\delta + d_2)}, \tag{2}$$

where $d_1 = |G_2|^2/\Gamma_{20} - i\delta + i\Delta_2$ and $d_2 = |G_2|^2/\Gamma_{20} - i\delta + i\Delta_1$. $G_i = \mu_{ij}E_i/\hbar$ are the Rabi frequency of $\boldsymbol{E_i}$, with the electric dipole matrix elements μ_{ij} of levels $|i\rangle$ and $|j\rangle$, and Γ_{ij} is the transverse decay rate. The linewidth of the measured SPFWM signal is $\Gamma = \Gamma_{10} + \Gamma_{00} + \Gamma_{20}$. $\delta = -(\Delta/2) \pm \Omega_e$ is the dressing bandwidth and Ω_e is effective Rabi frequency. Similarly, the density matrix for the Stokes and anti-Stokes in the two-level system can be written via $\rho_{00}^{(0)} \xrightarrow{E_1(\Delta_1)} \rho_{10}^{(1)} \xrightarrow{E_{AS}} \rho_{00}^{(2)} \xrightarrow{E_{1*}(\Delta_{1*})} \rho_{10(S)}^{(3)}$ as

$$\rho_{10}^{(3)} = \frac{-iG_S G_{1*} G_1}{(\Gamma_{10} + i\Delta_{1*})(\Gamma_{10} + i\delta)(\Gamma_{10} + i\delta - i\Delta_1 + |G_{1*}|^2/\Gamma_{00} + i\delta - \Delta_1 + d_3)} \tag{3}$$

$$\rho_{10}^{(3)} = \frac{-iG_{AS} G_{1*} G_1}{(\Gamma_{10} + i\Delta_1)(\Gamma_{10} + i\delta)(\Gamma_{00} - i\delta + i\Delta_1 + (|G_{1*}|^2/\Gamma_{00} + i\delta - \Delta_1 + d_4)}, \tag{4}$$

where $d_3 = |G_1|^2/\Gamma_{10} + i\delta$ and $d_4 = |G_1|^2/\Gamma_{10} + i\delta$. The linewidth of the measured SP FWM signal is $\Gamma = 2\Gamma_{10} + \Gamma_{00}$. The optical response of the medium in the two-level system produces three different FWM processes. A schematic diagram for one out of three FWMs is illustrated in figure 1(d). The temporal intensity of the Stokes and anti-Stokes signals is given by [8]

$$\langle I_S \rangle = e^{-2\Gamma_{00}t_S} + e^{-2\Gamma_{10}t_{AS}} - 2\cos(-\Delta_2 t_S)e^{-(\Gamma+\Gamma_{20})t_S} \tag{5}$$

$$\langle I_{AS} \rangle = e^{-2\Gamma_{00}t_{AS}} + e^{-2\Gamma_{20}t_S} - 2\cos(-\Delta_1 t_{AS})e^{-(\Gamma+\Gamma_{10})t_{AS}}. \tag{6}$$

The two-mode intensity noise correlation between the output Stokes and anti-Stokes SPFWM fields with time delay τ is given by can be obtained from

$$G^{(2)}(\tau) = \langle \delta I_S(t_S) \rangle \langle \delta I_{AS}(t_{AS}) \rangle$$
$$W_1 \ [e^{-2\Gamma_{e+}\tau_1} + e^{-2\Gamma_{e-}\tau_1} - 2\cos(\Omega_e \tau_1)e^{-(\Gamma_{e+}+\Gamma_{e-})\tau_1}], \tag{7}$$

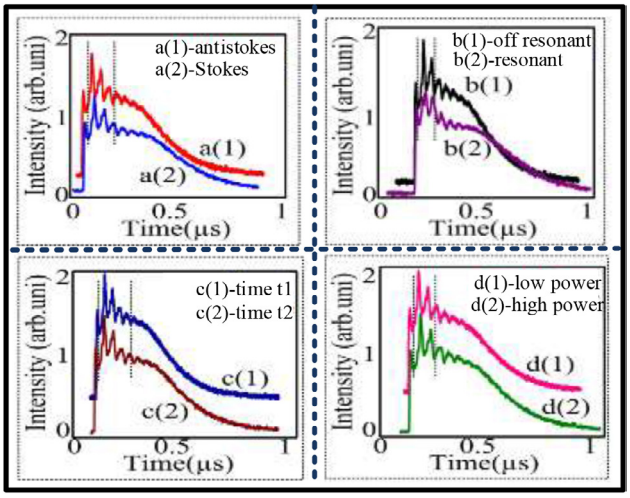

Figure 2. The comparison of the self-Rabi oscillations from (a) the temporal intensity of the Stokes and anti-Stokes signals (b) obtained from resonant and off-resonant excitations. (c) and (d) The dependence of the Rabi oscillation at different gate positions (t_1 and t_5) and the power of the input laser beam, respectively.

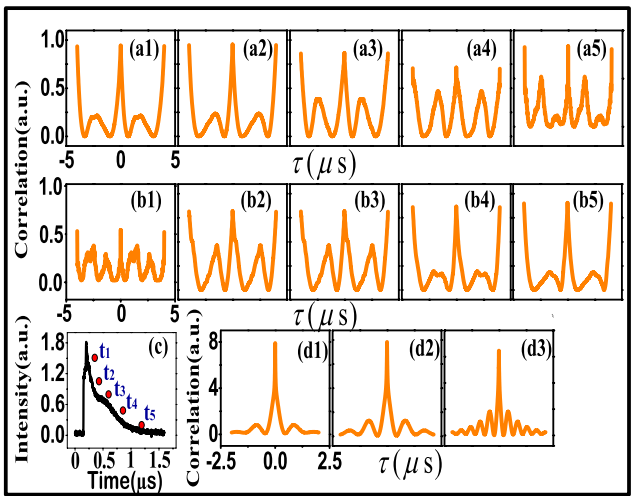

Figure 3. (a1)–(a5) Intensity noise correlation curves between $\boldsymbol{E}_{\mathbf{S}}$ and $\boldsymbol{E}_{\mathbf{AS}}$ versus the delayed time τ with a changing power of $\boldsymbol{E}_{\mathbf{1}}$. (b1)–(b5) Two-mode correlation by changing the position of the boxcar gate of the left peak signal from t_1 to t_5 (see figure (c)). (c) Setting the gate at different positions of peak intensities. (d1)–(d3) Theoretical simulation results show the Rabi oscillation's power is varied from high to low.

where $\Gamma_{e\pm} = (\Gamma_{00} + \Gamma_{10})/2 \pm (\Delta_1\Gamma_{10})/2\Omega_e$ is the decoherence rate. $\delta I_{\mathrm{AS}}(t_{\mathrm{AS}})$ and $\delta I_{\mathrm{S}}(t_{\mathrm{S}})$ are the intensity fluctuations of the $\boldsymbol{E}_{\mathbf{AS}}$ and $\boldsymbol{E}_{\mathbf{S}}$ signals, respectively.

3. Results and discussion

Figure 2(a) shows the temporal intensity of the Stokes and anti-Stokes signals detected by PMT1 and PMT3, respectively. The intensities of the Stokes and anti-Stokes signals present damped self-Rabi oscillations. Damped self-Rabi oscillations can be attributed to the quantum interference of two FWM transition paths. The intensity function mentioned in equations (5) and (6) shows cosine oscillation in time and is exponentially damped. With the detection of the SPFWM, the second order FL ($\rho_{11}^{(2)} = -G_1^2/[(\Gamma_{10} + i\Delta_1 + |G_1|^2/\Gamma_{11})\Gamma_{11}]$) is recorded in the PMTs. The decay rate of the FL signal is given by $\Gamma_{FL} = \Gamma_{10} + \Gamma_{11}$

Equations (5) and (6) show the Rabi oscillation frequency is determined by the detuning Δ of the incident beam and the damping rate Γ. From equation (5) we can obtain the Rabi oscillation frequency of the Stokes signal at Δ_2 with a damping rate of $\Gamma = \Gamma_{00} + \Gamma_{20}$. Unlike the Stokes signal, the Rabi oscillation frequency of the anti-Stokes signal is Δ_1 with a damping rate of $\Gamma = \Gamma_{00} + \Gamma_{10}$. The anti-Stokes photon has higher energy and larger detuning $\Delta_1 > \Delta_2$ than the Stokes photon. Therefore, the Rabi oscillation frequency in the anti-Stokes (figure 2(a1)) emission is higher than that of the Stokes (figure 2(a2)) emission. In figure 2(b), we study the dependence of Rabi oscillations on resonant (637 nm) and off-resonant (575 nm) excitations. After precisely measuring the periods of Rabi oscillations, we find that, for off-resonant excitation, the Rabi period of the Stokes signal is 65 ns, while, for resonant excitation, the Rabi period is 75 ns. Hence, we can conclude that the frequency of the Rabi oscillation is higher for a 575 nm excitation (figure 2(b1)) than a 637 nm excitation (figure 2(b2)). In figure 2(c), we study the dependence of the Rabi oscillation on the different gate positions t_1 and t_4 (see figure 3(d)). The signal that was observed at time t_1 (figure 3(c1)) has the dominant SPFWM emission, due to the particle transfer between the $|m_s = 0\rangle$ state. When the gate position is fixed at t_4 (figure 3(c2)), the FL emission increases more dramatically than the SPFWM. Hence, the dominant SPFWM emission at time t_1 results in a higher Rabi oscillation. In figure 2(d), we study the behavior of the Rabi oscillation when the power of $\boldsymbol{E}_{\mathbf{1}}$ (575 nm) is changed from low (1 mW) to high (7 mW). When the laser power of $\boldsymbol{E}_{\mathbf{1}}$ is set low (figure 2(d1)), the particle transfer via the direct path $|m_s = 0\rangle$ is high, which greatly enhances the SPFWM emission; whereas the dipole assisted transition (FL emission) from $|m_s = \pm 1\rangle$ significantly increases in competition to the SPFWM emission at a high power (figure 2(d2)). Hence, we can conclude that the strong SPFWM emission at a low power of $\boldsymbol{E}_{\mathbf{2}}$ results in a high frequency of self-Rabi oscillation, compared to the high power shown in figure 2(d1). To distinguish the self-Rabi oscillations (the interference between two linear decay processes in figure 2), next we will discuss the cross-Rabi oscillations (figures 3–5), which comes from the destructive interference of two nonlinear FWM processes.

Figures 3(a1)–(a5) shows the two-mode intensity noise correlation of Stokes/anti-Stokes and FL composite signals when the power (mW) of the $\boldsymbol{E}_{\mathbf{1}}$ (575 nm) input beam decreases from high (7 mW) to low (1 mW). The correlation function is calculated by the time-dependent intensity fluctuation described by equation (7). Using equation (7), the cross-Rabi frequency Ω_e can be written as $\Omega_e = \sqrt{\Delta_1^2 + 4(G_{1*}/G_1)^2\Gamma_{10}\Gamma_{00} + G_1^2}$, where G_1 and G_{1*} are dressing fields. In order to understand the cross-Rabi oscillation in the intensity correlation, we use the double dressing effect of the $\boldsymbol{E}_{\mathbf{1}}$ and $\boldsymbol{E}_{\mathbf{1}*}$ beams. The dressing effect can be used to control the frequency and amplitude

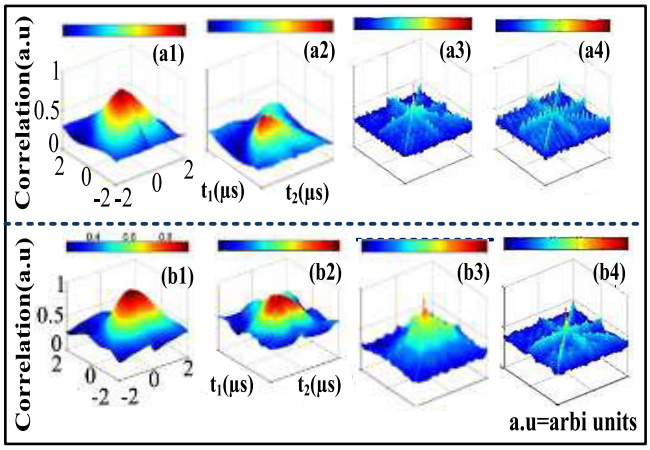

Figure 4. (a1)–(a4) and (b1)–(b4) shows the three-mode noise correlation of the $\boldsymbol{E}_{\mathbf{S}}$, $\boldsymbol{E}_{\mathbf{AS}}$ and FL signal in the two- and three-level (V-type) systems, respectively.

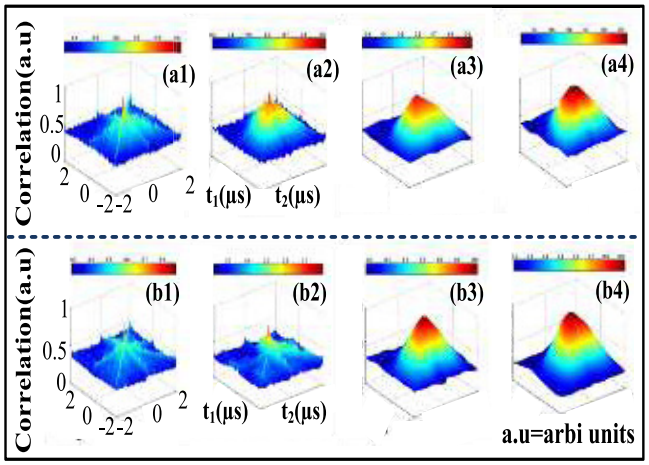

Figure 5. (a1)–(a4) and (b1)–(b4) shows the three-mode intensity noise correlation measured by changing the time position of the boxcar gate (see figure 3(c) in a two and V-type system).

of cross-Rabi oscillations [19]. In the case of a single dressing field, the FL signal increases gradually with the increasing power of the input field. When the power is further increased the FL signal evolves from a dressing state to suppression caused by the dressing effect of $\boldsymbol{E_1}$. With a further suppression of the FL signal, the SPFWM emission is enhanced gradually at a high power. However, in the double dressing scenario, the dressing effect dependence on the power is slightly reversed. When the power of the $\boldsymbol{E_1}$ dressing field is set high (7 mW), the frequency of the Rabi oscillation Ω_e is low due to the dominant dressing effect in equation (3), as shown by figure 3(a1). Furthermore, the intensity $I \propto \left|\rho^{(3)}_{10(AS)}\right|^2$ of the SP FWM is low at a high laser power, which results in a weak interference between two FWMs. The weak interference between two FWM processes produces the low frequency of Rabi oscillations. As the power of $\boldsymbol{E_1}$ decreases to 1 mW, the frequency of the Rabi oscillation increases due to the dominant gain and reduced dressing effect of dressing terms in equation (3), as shown in figure 3(a5). The intensity of the SP FWM increases at a low laser power, which results in the strong interference between two FWMs and the frequency of the Rabi oscillation increases.

Correlation curves in figures 3(b1)–(b5) are plotted for the different positions t_1–t_5 of the boxcar gate labeled in figure 3(c). When the gate position is at time position t_1, the SPFWM signal is dominant in the composite channel, as the Stokes and anti-Stokes signals are strong due to the high population transfer between the $|m_s = 0\rangle$ state. Hence, the composite channel acts like a pure SPFWM channel when the gate position is set to t_1. Due to the high emission of the SPFWM, the frequency of the Rabi oscillations is high, as seen in figure 3(b1). Further, by increasing the delay time, i.e. locating the gate position at t_5, the SPFWM signals vanish in the composite signal, owing to its fast decay rate relative to the slow decay rate of the FL and the composite signal becomes a pure FL signal. The FL emission in this case is caused by the phonon-assisted transition from the $|m_s = \pm 1\rangle$ state. Due to the high emission of the FL signal and the lower SPFWM output in the composite channel, it greatly reduces the interference between recorded outputs, resulting in the decrease in frequency of Rabi oscillations, plotted in figure 3(b5).

In the two-mode intensity correlation, the shape of the correlation function for the composite (FL + SPFWM) signal is determined by $A_c = R_1|A_1|^2[e^{-2(\Gamma_1^+ + \Gamma_2^+ + \zeta)|\tau|} + e^{-2(\Gamma_1 + \Gamma_2 + \zeta)|\tau|} - 2\cos(\Omega_e|\tau|)e^{-2(\Gamma_1^+ + \Gamma_2^+ + \Gamma_1^- + \Gamma_2 + \zeta)|\tau|}$, where $R_1 = N|\mu_{ij}\mu_{kl}|\omega_{s/as}E_1^2 L[2c\varepsilon_0 h^3(\Gamma_{10} + i\Delta^*_{1/2})]$. From equations (5)–(7), we can conclude that the line shape and frequency of the cross-Rabi oscillation Ω_e is independent to the amplitude and frequency of the self-Rabi oscillation. However, the amplitude of the cross-Rabi oscillation is affected by the frequency of the self-Rabi oscillation. Figure 3(c) shows the selected gate position in the time domain intensity signal. Figures 3(d1)–(d3) show the theoretical results of the Rabi oscillations, which correspond to our experimental results in figures 3(a1), (a3) and (a5).

Figure 4 shows the measured three-mode intensity noise correlation of Stokes, anti-Stokes and FL composite signals detected in the setup shown in figure 1(c). The intensity fluctuations $\delta I_1(t_1)$, $\delta I_2(t_2)$ and $\delta I_3(t_3)$ are recorded and the triple beam intensity correlation is plotted using $G^{(3)}_{cc}(\tau) = \langle \delta I_1(t_1)\delta I_2(t_2)\delta I_3(t_3)\rangle$. The power dependence of the Rabi oscillations for $G^{(3)}_{cc}(\tau)$ is similar to the two-intensity correlation, which is explained in figure 3(a). The Rabi oscillation frequency is low when the power of the dressing field is high and vice versa. Figures 4(b1)–(b4) show the experimental results of the three-mode correlation in the V-type system. The total intensity of the hybrid signal is given by $\rho = \rho_{\mathrm{FL}} + \rho_{\mathrm{SPFWM}}$ where $\rho_{FL} = \rho^{(4)}_{22}$ and $\rho_{\mathrm{SPFWM}} = \rho^{(3)}_{\mathrm{S/AS}}$. When the power of $\boldsymbol{E_1}$ is set at 7 mW, the frequency of the Rabi oscillation $\Omega_e = \sqrt{\Delta_1^2 + 4(G_1/G_2)^2\Gamma_{10}\Gamma_{00} + G_1^2}$ is low due to the strong dressing effect $|G_2|^2/\Gamma_{00} - i\delta$ and the low SPFWM emission (equation (1*a*)) shown by figure 4(b1). When the power is reduced, the dressing effect decreases and the SPFWM emission increases due to the high gain effect of G_2 of $\boldsymbol{E_2}$, explained by equation (1). The frequency of the Rabi

oscillation increases due to the strong interference between two SPFWMs, as seen in figure 4(b4).

The three-mode intensity correlation in figure 5 is experimentally measured for different positions (t_1–t_5) of the boxcar gate labeled in figure 3(c). Figure 5 shows a similar dependence on the gate position, as observed in figure 3(b). When the gate position is at t_1, the SPFWM emission is strong, which leads to the high frequency of Rabi oscillations seen in figure 5(a1). By increasing the time delay to t_5, the FL emission increases, and the frequency of the Rabi oscillation decreases, as shown in figure 5(a4). Figures 5(b1)–(b4) show the three-mode correlation in the V-type system, which corresponds to the similar behavior of the cross-Rabi oscillation with a two-level system.

In figure 4, the Rabi oscillations are more prominent in the two-level system (figure 4(a)) because of the strong dressing effect of the input field $\boldsymbol{E_{1*}}$. However, in figure 5, with an introduction of the resonant beam $\boldsymbol{E_1}$, the particle transfer from the $|m_s = 0\rangle$ state increases along with a strong SPFWM emission. Hence, the frequency of the Rabi oscillations increases, as shown in figure 5(b).

Conclusion

In conclusion, we studied the relationship between the temporal intensity self-Rabi oscillations and the intensity noise cross-Rabi oscillations. The self and cross-Rabi oscillations come from the interference of two linear decay and two nonlinear FWM processes, respectively. Two mode and three mode cross-Rabi oscillation can be controlled by the dressing power and boxcar gate position. Such Rabi oscillations in the NV center may have potential applications in quantum lithography [14].

Acknowledgments

This work was supported by the National Key R&D Program of China (2017YFA0303703, 2018YFA0307500), National Natural Science Foundation of China (11474228, 61605154, 11604256).

References

[1] Harris S 1997 Laser without inversion: interference of lifetime-broadened *Phys. Today* **50** 36–42
[2] Braje D A, Balic V, Goda S, Yin G Y and Harris S E 2004 Frequency mixing using electromagnetically induced transparency in cold atoms *Phys. Rev. Lett.* **93** 183601
[3] Gisin N, Grégoire R, Wolfgang T and Hugo Z 2002 Quantum cryptography *Rev. Mod. Phys.* **74** 145
[4] Neilson M and Chuang I 2002 Quantum computation and quantum information *Am. J. Phys.* **70** 558
[5] Saleh B E, Bradley M J, Hong-Bing F and Malvin C T 1998 Entangled-photon virtual-state spectroscopy *Phys. Rev. Lett.* **80** 3483
[6] Jianming W, Shengwang D and Morton H R 2007 Biphoton generation in a two-level atomic ensemble *Phys. Rev.* A **75** 033809
[7] Shengwang D, Oh E, Jianming W and Morton H R 2007 Four-wave mixing in three-level systems: interference and entanglement *Phys. Rev.* A **76** 013803
[8] Shengwang D, Jianming W, Morton H R and Yin G Y 2007 Four-wave mixing and biphoton generation in a two-level system *Phys. Rev. Lett.* **98** 053601
[9] Gruber A, Dräbenstedt A, Tietz C, Fleury L, Wrachtrup J and Borczyskowski C V 1997 Scanning confocal optical microscopy and magnetic resonance on single defect centers *Science* **276** 2012–4
[10] Dutt M V G, Childress L, Jiang L, Togan E, Maze J, Jelezko F, Zibrov A S, Hemmer P R and Lukin M D 2007 Quantum register based on individual electronic and nuclear spin qubits in diamond *Science* **316** 1312–6
[11] Bar-Gill N, Linh M P, Andrejs J, Dmitry B and Ronald L W 2013 Solid-state electronic spin coherence time approaching one second *Nat. Commun.* **4** 1743
[12] Kurtsiefer C, Mayer S, Zarda P and Weinfurter H 2000 Stable solid-state source of single photons *Phys. Rev. Lett.* **85** 290
[13] Jelezko F, Gaebel T, Popa I, Domhan M, Gruber A and Jorg W 2004 Observation of coherent oscillation of a single nuclear spin and realization of a two-qubit conditional quantum gate *Phys. Rev. Lett.* **93** 130501
[14] Liao Z, Al-Amri M and Zubairy M S 2010 Quantum lithography beyond the diffraction limit via Rabi oscillations *Phys. Rev. Lett.* **105** 183601
[15] Batalov A, Zierl C, Gaebel T, Neumann P, Chan I Y, Balasubramanian G, Hemmer P R, Jelezko F and Wrachtrup J 2008 Temporal coherence of photons emitted by single nitrogen-vacancy defect centers in diamond using optical Rabi-oscillations *Phys. Rev. Lett.* **100** 077401
[16] Schirhagl R, Chang K, Loretz M and Degen C L 2014 Nitrogen-vacancy centers in diamond: nanoscale sensors for physics and biology *Annu. Rev. Phys. Chem.* **65** 83–105
[17] Zhang Y, Brown A W and Xiao M 2007 Opening four-wave mixing and six-wave mixing channels via dual electromagnetically induced transparency windows *Phys. Rev. Lett.* **99** 123603
[18] Zhang Y, Khadka U, Anderson B and Xiao M 2009 Temporal and spatial interference between four-wave mixing and six-wave mixing channels *Phys. Rev. Lett.* **102** 013601
[19] Lan H, Li C, Lei C, Zheng H, Wang R, Xiao M and Zhang Y 2014 Competition between spontaneous parametric four-wave mixing and fluorescence in Pr^{3+}:YSO *Laser Phys. Lett.* **12** 015404